THE JOURNAL OF PHYSICAL CHEMISTRY Letters

Letter

pubs.acs.org/JPCL

Mechanism for Broadband White-Light Emission from Two-Dimensional (110) Hybrid Perovskites

Te Hu,[†,‡] Matthew D. Smith,[§] Emma R. Dohner,[§] Meng-Ju Sher,[‡] Xiaoxi Wu,[†] M. Tuan Trinh,[∥] Alan Fisher,[⊥] Jeff Corbett,[⊥] X.-Y. Zhu,[∥] Hemamala I. Karunadasa,[*,§] and Aaron M. Lindenberg[*,†,‡,▽]

[†]Stanford Institute for Materials and Energy Sciences, SLAC National Accelerator Laboratory, Menlo Park, California 94025, United States

[‡]Department of Materials Science and Engineering, Stanford University, Stanford, California 94305, United States

[§]Department of Chemistry, Stanford University, Stanford, California 94305, United States

[∥]Department of Chemistry, Columbia University, New York, New York 10027, United States

[⊥]SLAC National Accelerator Laboratory, Menlo Park, California 94025, United States

[▽]PULSE Institute, SLAC National Accelerator Laboratory, Menlo Park, California 94025, United States

Supporting Information

ABSTRACT: The recently discovered phenomenon of broadband white-light emission at room temperature in the (110) two-dimensional organic–inorganic perovskite (*N*-MEDA)[$PbBr_4$] (*N*-MEDA = N^1-methylethane-1,2-diammonium) is promising for applications in solid-state lighting. However, the spectral broadening mechanism and, in particular, the processes and dynamics associated with the emissive species are still unclear. Herein, we apply a suite of ultrafast spectroscopic probes to measure the primary events directly following photoexcitation, which allows us to resolve the evolution of light-induced emissive states associated with white-light emission at femtosecond resolution. Terahertz spectra show fast free carrier trapping and transient absorption spectra show the formation of self-trapped excitons on femtosecond time-scales. Emission-wavelength-dependent dynamics of the self-trapped exciton luminescence are observed, indicative of an energy distribution of photogenerated emissive states in the perovskite. Our results are consistent with photogenerated carriers self-trapped in a deformable lattice due to strong electron–phonon coupling, where permanent lattice defects and correlated self-trapped states lend further inhomogeneity to the excited-state potential energy surface.

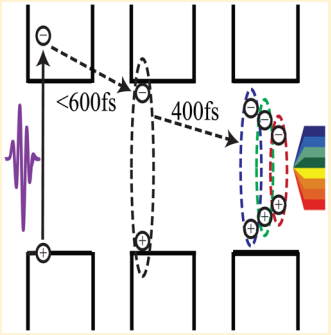

Organic–inorganic perovskites show diverse and technologically important optoelectronic properties that can be systematically tuned through the dimensionality of the inorganic framework. Three-dimensional hybrid lead-halide perovskites (CH_3NH_3)[PbX_3] (X = Br and I) have gained prominence recently as efficient absorbers in photovoltaic cells.[1,2] These materials exhibit a narrow luminescence peak at the bandgap energy and a number of studies have been focused on their applications as light-emitting diodes and as laser gain media.[3−6] In the two-dimensional limit, additional novel optical and functional properties emerge.[7−10] For example, two-dimensional lead-iodide perovskites have been shown to function as absorbers in solar cells with high open-circuit voltages,[7] and narrow photo- and electroluminescence have been achieved in lead-halide perovskites.[8,9] In prior work, we showed that the (110) two-dimensional hybrid perovskites (*N*-MEDA)[$PbBr_4$] (*N*-MEDA = N^1-methylethane-1,2-diammonium) and (EDBE)[PbX_4] (EDBE = 2,2′-(ethylenedioxy)bis(ethylammonium); X = Cl and Br) exhibit broadband white-light emission upon near-ultraviolet excitation at room temperature.[11,12] The emitted white light has color rendering indices exceeding commercial requirements for indoor illumination, and both "warm" and "cold" white light can be achieved by halide substitution, important for applications in solid-state lighting. We proposed that this novel broadband white-light emission arises from self-trapped excitons (STEs) as well as from carriers trapped at permanent defects.[11,12] In contrast to permanent material defects (such as lattice vacancies), STEs are transient defects that form in the excited state where photogenerated charge carriers are stabilized through large lattice distortions driven by strong electron–phonon coupling.[13] A time-resolved photoluminescence (PL) study on a related white-light-emitting (001) two-dimensional perovskite has been recently reported.[14] However, the dynamics that immediately follow photoexcitation have not been studied to date. Investigation of the microscopic processes and ultrafast dynamics associated with events that immediately follow photoexcitation is critical toward understanding the self-trapping process, which may guide the design of new broadband white-light emitters with optimized functionality.

There are a number of examples of broadband light emission in materials with strong electron–phonon interactions.[15−19] In

Received: April 13, 2016
Accepted: June 1, 2016

DOI: 10.1021/acs.jpclett.6b00793
J. Phys. Chem. Lett. 2016, 7, 2258−2263

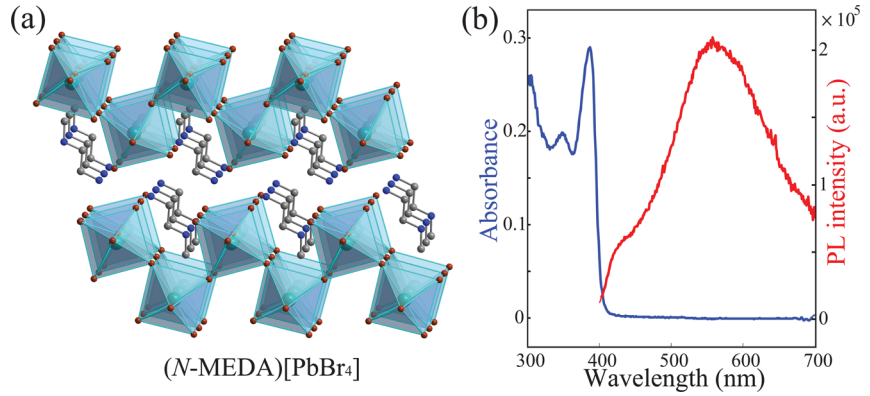

Figure 1. (a) Crystal structure of the (110) perovskite (*N*-MEDA)[$PbBr_4$].[11] Turquoise, brown, blue, and gray spheres represent Pb, Br, N, and C atoms, respectively. H atoms are omitted for clarity. (b) Static optical absorption spectrum (blue) of a film of (*N*-MEDA)[$PbBr_4$] measured using an integration sphere to eliminate diffuse scattering and emission spectrum of a powder sample (red).

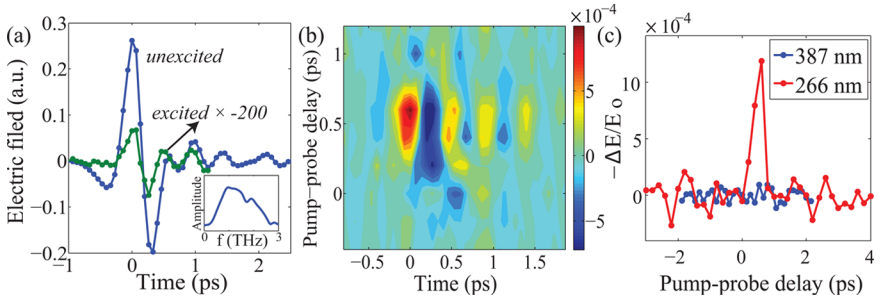

Figure 2. (a) THz waveform transmitted through an unexcited thin film (blue) and the waveform change (green) measured at 600 fs after 266 nm photoexcitation. The inset shows the frequency domain (0.5−2.5 THz) of the transmitted THz pulse. (b) Two-dimensional waveform change as a function of the pump−probe delay and electro-optic sampling delay. (c) Relative change in the peak of the THz transmission ($-\Delta E/E_0$, E_0 is the peak electric field amplitude of the THz pulse transmitted through an unexcited film) under two different excitation wavelengths. The excitation fluence is 50 $\mu J/cm^2$ (6.7×10^{13} photons/cm^2/pulse).

these materials, photogenerated free carriers typically first form free excitons, which then relax into STEs with an associated surrounding lattice deformation. Luminescence from the STEs gives rise to broadband Stokes-shifted emission. STE formation is found to have a strong dependence on the dimensionality of the system.[20−22] In the one-dimensional limit there is no potential barrier separating the free exciton and STE, and thus, the STE forms promptly, on subpicosecond time-scales, from the free exciton.[15−17,23] In the three-dimensional systems, STE formation typically takes significantly longer (~2 ns in RbI single crystals) due to the existence of a large potential barrier for trapping.[19] Two-dimensional systems are thought to be an intermediate case, where modeling predicts two critical thresholds for the electron−phonon coupling constant, above which self-trapping may occur with or without an energy barrier.[20,21] In this work, we study the hybrid perovskite (*N*-MEDA)[$PbBr_4$], which is the first reported white-light emitter in the two-dimensional hybrid perovskite family and has a PL quantum efficiency (PLQE) of ~0.5% at room temperature.[11] We apply ultrafast terahertz (THz), optical transient absorption (TA), and PL spectroscopy to directly resolve the initial events from excitation of free charges to free exciton formation to STE formation, resolving the dynamics of the emissive states associated with white-light emission. We show that STEs form in a quasibarrierless manner (barrier height <4 meV) and that broadband emission is associated with an ensemble of transient light-induced emissive states developing on subpicosecond time-scales.

The perovskite (*N*-MEDA)[$PbBr_4$] adopts a layered structure (Figure 1a) with corrugated inorganic lead-bromide sheets separated by organic cations (molecular structures shown in Figure S1).[11] This results in a natural multiquantum well-like electronic structure.[24] Figure 1b shows the static optical absorption spectrum of an (*N*-MEDA)[$PbBr_4$] thin film with crystallinity confirmed by grazing-incidence X-ray diffraction measurement[25] (Figure S3). A sharp exciton peak occurs at 387 nm with a binding energy of ~0.3 eV, estimated as the difference between the bandgap and excitonic absorption peak in the low-temperature (5 K) absorption spectrum (not shown here). Following above-excitonic-peak photoexcitation, the broadband PL is centered at ~560 nm and spans the entire visible spectrum.[11]

To probe the dynamics of free carriers after photoexcitation,[26−28] time-resolved THz measurements were performed on (*N*-MEDA)[$PbBr_4$] thin films. The reference THz waveform transmitted through an unexcited thin film is shown in Figure 2a, together with the waveform change measured at 600 fs after 266 nm above-gap photoexcitation. The 266 nm pump-induced change in the transmitted THz electric field was measured at variable pump−probe delays producing the two-dimensional time-domain data shown in Figure 2b. The change in the transmitted THz electric field signifies the onset of transient photoconductivity in the sample, which reaches its maximum ~600 fs after photoexcitation and recovers almost instantaneously, limited by the time resolution of the setup. As the product of the electric charge, charge carrier mobility, and the density of photogenerated free carriers,[29] measurement of

DOI: 10.1021/acs.jpclett.6b00793
J. Phys. Chem. Lett. 2016, 7, 2258−2263

the transient photoconductivity provides a direct monitor of the density of photogenerated free carriers in this wide bandgap material. Its rapid turn on and turn off indicate a similarly rapid free carrier generation under 266 nm photoexcitation, followed by an immediate removal of free carriers from the conduction band. Note this measurement alone does not distinguish between free carriers that evolve into free excitons or to STEs or distinguish between STE formation and trapping at permanent defects. Figure 2c compares the differential THz transmission ($-\Delta E/E_0$) as a function of the pump−probe delay under 266 and 387 nm (in resonance with the exciton) photoexcitation. No transient photoconductivity, and therefore no photogenerated free carriers, are observable under 387 nm pump, indicating the direct formation of excitons in the sample under resonant exciton pumping, consistent with the large exciton binding energy of (*N*-MEDA)[$PbBr_4$].

To probe the electronic trap states associated with the broadband emission following free exciton formation, below-gap TA spectroscopy was measured on (*N*-MEDA)[$PbBr_4$] thin films with 387 nm resonant exciton pumping and white-light supercontinuum probes, as shown in Figure 3. Following

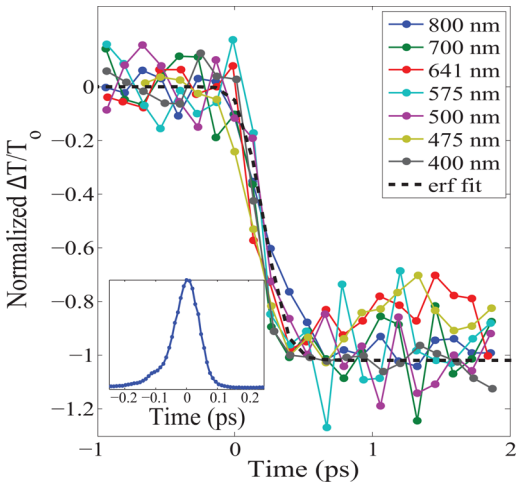

Figure 3. Normalized TA onsets probed at below-gap wavelengths under 387 nm resonant photoexcitation at room temperature for (*N*-MEDA)[$PbBr_4$]. The inset shows the response function of the setup measured by cross-correlation of the white-light supercontinuum with 800 nm laser light. The excitation fluence is 50 $\mu J/cm^2$ (9.7×10^{13} photons/cm^2/pulse).

387 nm photoexcitation, a broad below-gap induced absorption feature is observed. This is in contrast to the reported TA spectra of two-dimensional and three-dimensional lead-iodide hybrid perovskites,[30] where broad below-gap bleaching features are observed as permanent defects in the below-gap region are populated by relaxed photogenerated charge carriers. Because of the negligible optical absorption in the below-gap energy region (Figures 1b and S2), permanent lattice defect states are not likely to play a dominant role here. This is consistent with prior studies in the analogous (110) perovskite (EDBE)[$PbBr_4$] where the integrated PL intensity shows a linear dependence on excitation intensity instead of a sublinear dependence as permanent defect states are filled.[12] Because no free carriers are generated with 387 nm resonant photoexcitation (Figure 2c), this feature cannot be explained by free carrier absorption. We attribute the observed induced absorption to the formation of new electronic states in the below-gap region following photoexcitation. The rapid turn-on time (~400 fs) is longer than the time resolution of the measurement (~90 fs), measured by a cross-correlation of the white-light supercontinuum with 800 nm femtosecond pulses (inset to Figure 3). This turn-on time is comparable to the period of the Pb−Br stretching mode (~300 fs) in (EDBE)[$PbBr_4$] as measured by Raman spectroscopy. This mode has been attributed to the phonon mode coupled to the electronic transition as revealed from the temperature dependence of the fwhm of the PL emission.[12] STE formation times comparable to the vibrational period of the relevant phonon mode have been observed in other 1D exciton self-trapping systems[23] and indicates that almost no potential barrier exists for the transition from free excitons to STEs. The almost identical rise time of all probing wavelengths indicates these new self-trapped states formed simultaneously within the resolution of our TA setup (~90 fs).

To further confirm that the pump-induced absorption is from self-trapped states rather than from free excitons or permanent lattice defects, we measured the (001) two-dimensional perovskite, (*N*-MPDA)[$PbBr_4$] (*N*-MPDA = N^1-methylpropane-1,2-diammonium; structure shown in Figure S1). As previously reported, instead of broad white-light emission, (*N*-MPDA)[$PbBr_4$] shows narrow free excitonic emission upon photoexcitation at room temperature (Figure S6a).[11] Contrary to (*N*-MEDA)[$PbBr_4$], instead of a pump-induced absorption, we observed only an induced increase in transmission near the lower-energy tail of the exciton band (Figure S6b). The absence of lower-energy absorption features in (*N*-MPDA)[$PbBr_4$] suggests that the self-trapped states associated with the broad emission have not formed in this narrow emitter. Similar responses were seen in a (001) lead-iodide perovskite and assigned to permanent trap states.[30]

Time-resolved PL spectroscopy was measured on (*N*-MEDA)[$PbBr_4$] single crystals and pressed-powder pellets to directly follow the evolution of the light-induced emissive states. Both samples give broadband emission and the PL spectra are similar to each other (Figure S7). As shown in Figure 4a, wavelength-dependent PL decay dynamics are observed at room temperature. The free exciton luminescence at 390 nm drops to $1/e$ of its maximum value on a time-scale limited by the experimental time resolution (~8 ps) whereas longer wavelengths decay on longer time-scales. Also shown in Figure 4a are fits to the measured PL decay using a stretched-exponential function $I(t) = I_0 \times \exp\{-(t/\tau)^{\beta}\}$, where τ and β are two fitting parameters.[31,32] This function is typically applied when a distribution of relaxation times are involved.[33] The fitted decay time-constants τ are summarized in Figure 4b, which exhibit an exponential dependence on the emitted photon energy. Similar emission-wavelength-dependent relaxation dynamics have been reported in studies of luminescence from Si nanocrystals embedded in SiO_2.[31,32] In these reports, the exponential dependence of PL decay dynamics on the emission energy has been attributed to nonradiative quenching of STE states through a phonon-assisted tunneling mechanism, with the tunneling probability for more deeply trapped states exponentially reduced. Wavelength-dependent PL decay times have also been recently reported in a related (001) lead-bromide perovskite, although the exponential form of this dependence or possible origins were not discussed.[14] Temperature-dependent PL-decay dynamics in (*N*-MEDA)[$PbBr_4$] selectively integrating over the peak STE emission (530−650 nm) show that the STE luminescence becomes longer (Figure S9) and more efficient (~75% PLQE at 20 K) at lower

DOI: 10.1021/acs.jpclett.6b00793
J. Phys. Chem. Lett. 2016, 7, 2258−2263

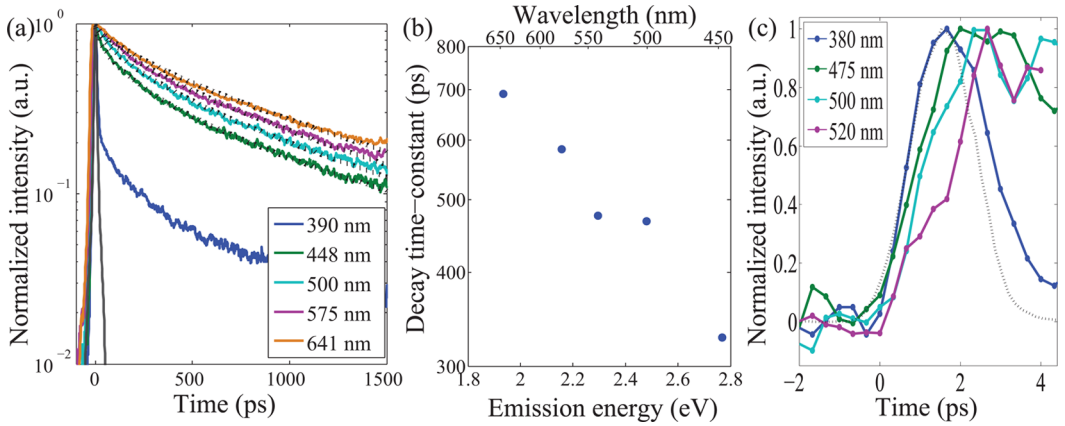

Figure 4. (a) Normalized PL decay of (*N*-MEDA)[$PbBr_4$] after 343 nm photoexcitation measured at various emission wavelengths at room temperature. The black dotted lines are fits to the result based on the equation described in the text, where both τ and β (~0.65) are allowed to vary to achieve the best fitting. The solid black line is the response function of the system. The excitation fluence is 13 $\mu J/cm^2$ (2.2×10^{13} photons/cm^2/pulse). (b) Spectral dependence of the decay time-constants obtained from the fitting. (c) Normalized PL onsets with 266 nm photoexcitation at room temperature.

temperatures, consistent with attenuation of nonradiative decay channels. Figure 4c shows the PL onset time measured using an optical Kerr-gate setup with ~1.3 ps time resolution (setup described in the Supporting Information) showing an ultrafast turn-on, consistent with the TA measurements. Although this measurement was carried out under much higher excitation fluence to obtain sufficient signal-to-noise (8 mJ/cm^2) and we expect competing dynamics of exciton−exciton annihilation, a similar spectral dependence of the PL turn-on dynamics is observed, with longer emission wavelengths evolving more slowly on few-picosecond time-scales.

To determine the potential barriers between free exciton and STE states, we measured the temperature-dependent ratio between free exciton and STE luminescence using a streak camera to capture the radiated photons from each of the two states (Figure 5a, details in the Supporting Information). With decreasing temperature, the STE luminescence becomes more dominant compared to free exciton luminescence, and the intensity ratio reaches a plateau below ~40 K. This trend has been observed in other materials and can be understood as arising from a thermally driven back transfer from the STE to the free exciton state, which becomes more difficult at lower temperatures.[34] The free exciton PL decay curve shows a rapid drop followed by a long tail (Figure S10). We interpret this as evidence for fast transfer from the free exciton to the STE state followed by a rapid thermal equilibrium established within picoseconds that sets the number of carriers in each state. The essentially linear response observed in both the PL (Figure S11) and TA (Figure S12) measurements as a function of fluence shows that at the intensities investigated here, exciton−exciton annihilation effects do not play a dominant role in the fast decay of the free exciton PL signal. The self-trapping depth (or difference in activation energies for carrier transfer between the free exciton and STE states) can then be obtained by fitting the measured PL intensity ratios as a function of temperature to the Arrhenius relation, shown as the red dotted line in Figure 5a, which gives a value of ~18 meV. Here, we assume equal nonradiative decay rates from the free exciton and STE states. At even lower temperatures (15−40 K), the STE formation from free excitons becomes limited, and the intensity ratio reaches a plateau, which may indicate that tunneling between the STE and free exciton states continues to be possible. Supporting Information Figure S10 shows that even at 17 K, a quasi-equilibrium exists between the free exciton and STE states, as shown by the roughly equal decay constants at long times. At sufficiently low temperatures (not measured here), the free exciton luminescence should be dominant over the STE luminescence (without considering the effects of tunneling), and the ratio of I_{STE}/I_{FE} (FE for free exciton) should decrease. Our measurements set an upper limit to the energy barrier for the free exciton to STE transition as approximately 4 meV. This is consistent with the fast turn-on of the induced absorption effect in TA measurements and the rapid onset of the STE PL.

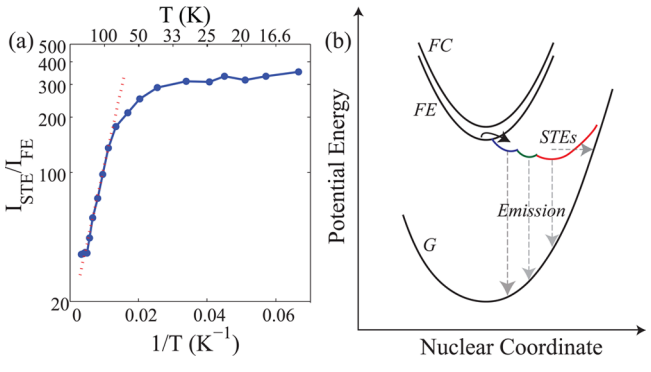

Figure 5. (a) Intensity ratio of STE and free exciton luminescence (I_{STE}/I_{FE}) as a function of temperature (blue) under 343 nm photoexcitation. The red dotted line is a linear fit to the curve. (b) Schematic of the adiabatic potential energy curves of the ground state (G), free-exciton state (FE), free-carrier state (FC), and various excited states (STEs) in a configuration space. The horizontal dashed line shows possible nonradiative decay processes of the STEs.

Several models have been proposed to explain intrinsic PL broadening.[17,35] One model considers carriers in a single excited state that is distorted with respect to the ground state relaxing into different vibrational levels in the ground state, giving rise to a homogeneously broadened emission peak.[35] Our measurements show wavelength-dependent PL onset and relaxation times (Figure 4), indicating that the emission broadening cannot be purely homogeneous and that there has to be a distribution of emissive self-trapped states. This is

DOI: 10.1021/acs.jpclett.6b00793
J. Phys. Chem. Lett. 2016, 7, 2258−2263

consistent with the observed stretched-exponential decay as well as the inhomogeneous contributions we previously used to model the temperature dependence of the emission width in the related (110) perovskite (EDBE)[$PbBr_4$].[12] We note that we can rule out the possibility that the broad emission originates from cooling of "hot" STEs to the excited-state potential surface minimum, which gives rise to a symmetric distribution of decay times around the emission peak wavelength,[15,16] not observed here. Our result is consistent with a model considering both the inhomogeneous nature of the STE states and their radiative and nonradiative decay, as illustrated in Figure 5b. In this model, a distribution of STE states with different self-trapping depths arises from free excitons through strong electron−phonon interactions. Longer emission wavelengths come from more distorted and deeper trapped emissive states, and excited carriers may shuttle from shallower trapped states to more deeply trapped states. As a result, PL in the red-end of the emission spectrum turns on more slowly, as observed in Figure 4c. We note that permanent lattice defects (such as vacancies) may also play a role here by adding further inhomogeneity to the excited-state potential surface and aiding the self-trapping process. Such defect-assisted, extrinsic self-trapping is commonly found in systems where intrinsic self-trapping is observed.[13] Furthermore, correlations between self-trapped states may serve a similar role to that of permanent lattice defects. For example, a large lattice distortion that follows an initial self-trapping event could serve as a transient nucleating site (akin to a permanent lattice defect) for a subsequent self-trapping event.

In conclusion, we have shown that the broadband Stokes-shifted emission in the two-dimensional (110) hybrid perovskite (*N*-MEDA)[$PbBr_4$] originates from a photogenerated energy distribution of STE states. Almost no potential barrier exists for the transition from free exciton to STE due to strong electron−phonon coupling, enabling ultrafast formation of the STE states as observed by both transient absorption and photoluminescence measurements. The distribution of self-trapped states likely arises from multiple local minima in the excited-state potential energy surface, with likely additional contributions from permanent material defects and correlated self-trapped sites. Additional information about the local structural reorganizations associated with the formation of these trap states may be obtained in the future through time-resolved X-ray/electron spectroscopy and scattering approaches.[36,37]

■ ASSOCIATED CONTENT

Supporting Information

The Supporting Information is available free of charge on the ACS Publications website at DOI: 10.1021/acs.jpclett.6b00793.

Experimental details, molecular structures of organic cations, grazing-incidence X-ray diffraction pattern, additional transient absorption and temperature-dependent PL studies, and fluence-dependent responses. (PDF)

■ AUTHOR INFORMATION

Corresponding Authors

*E-mail: hemamala@stanford.edu.

*E-mail: aaronl@stanford.edu.

Notes

The authors declare no competing financial interest.

■ ACKNOWLEDGMENTS

This work was supported by the Precourt Institute for Energy at Stanford University. Terahertz spectroscopic studies and X-ray characterization were supported by the Department of Energy, Basic Energy Sciences, Materials Sciences and Engineering Division. Grazing incidence X-ray diffraction studies were performed at the Stanford Synchrotron Radiation Lightsource (SSRL). Use of the Stanford Synchrotron Radiation Lightsource, SLAC National Accelerator Laboratory, is supported by the U.S. Department of Energy, Office of Science, Office of Basic Energy Sciences under Contract No. DE-AC02-76SF00515. H.K. acknowledges the Alfred P. Sloan Fellowship and the Stanford Terman Fellowship for research support. M.S. acknowledges an NSF graduate fellowship (No. DGE-114747) and additional support from the Global Climate and Energy Project. X.-Y.Z. acknowledges support from the U.S. Air Force Office of Scientific Research grant number FA9550-14-1-0381.

■ REFERENCES

(1) Kojima, A.; Teshima, K.; Shirai, Y.; Miyasaka, T. Organometal Halide Perovskites as Visible-Light Sensitizers for Photovoltaic Cells. *J. Am. Chem. Soc.* **2009**, *131*, 6050−6051.

(2) Snaith, H. J. Perovskites: The Emergence of a New Era for Low-Cost, High-Efficiency Solar Cells. *J. Phys. Chem. Lett.* **2013**, *4*, 3623−3630.

(3) Xing, G.; Mathews, N.; Lim, S. S.; Yantara, N.; Liu, X.; Sabba, D.; Grätzel, M.; Mhaisalkar, S.; Sum, T. C. Low-Temperature Solution-Processed Wavelength-Tunable Perovskites for Lasing. *Nat. Mater.* **2014**, *13*, 476−480.

(4) Deschler, F.; Price, M.; Pathak, S.; Klintberg, L. E.; Jarausch, D.-D.; Higler, R.; Hüttner, S.; Leijtens, T.; Stranks, S. D.; Snaith, H. J.; et al. High Photoluminescence Efficiency and Optically Pumped Lasing in Solution-Processed Mixed Halide Perovskite Semiconductors. *J. Phys. Chem. Lett.* **2014**, *5*, 1421−1426.

(5) Tan, Z.-K.; Moghaddam, R. S.; Lai, M. L.; Docampo, P.; Higler, R.; Deschler, F.; Price, M.; Sadhanala, A.; Pazos, L. M.; Credgington, D.; et al. Bright Light-Emitting Diodes Based on Organometal Halide Perovskite. *Nat. Nanotechnol.* **2014**, *9*, 687−692.

(6) Zhu, H.; Fu, Y.; Meng, F.; Wu, X.; Gong, Z.; Ding, Q.; Gustafsson, M. V.; Trinh, M. T.; Jin, S.; Zhu, X. Lead Halide Perovskite Nanowire Lasers with Low Lasing Thresholds and High Quality Factors. *Nat. Mater.* **2015**, *14*, 636−642.

(7) Smith, I. C.; Hoke, E. T.; Solis-Ibarra, D.; McGehee, M. D.; Karunadasa, H. I. A Layered Hybrid Perovskite Solar-Cell Absorber with Enhanced Moisture Stability. *Angew. Chem., Int. Ed.* **2014**, *53*, 11232−11235.

(8) Era, M.; Morimoto, S.; Tsutsui, T.; Saito, S. Organic−Inorganic Heterostructure Electroluminescent Device Using a Layered Perovskite Semiconductor $(C_6H_5C_2H_4NH_3)_2PbI_4$. *Appl. Phys. Lett.* **1994**, *65*, 676−678.

(9) Chondroudis, K.; Mitzi, D. B. Electroluminescence from an Organic−Inorganic Perovskite Incorporating a Quaterthiophene Dye within Lead Halide Perovskite Layers. *Chem. Mater.* **1999**, *11*, 3028−3030.

(10) Dou, L.; Wong, A. B.; Yu, Y.; Lai, M.; Kornienko, N.; Eaton, S. W.; Fu, A.; Bischak, C. G.; Ma, J.; Ding, T.; et al. Atomically Thin Two-Dimensional Organic-Inorganic Hybrid Perovskites. *Science* **2015**, *349*, 1518−1521.

(11) Dohner, E. R.; Hoke, E. T.; Karunadasa, H. I. Self-Assembly of Broadband White-Light Emitters. *J. Am. Chem. Soc.* **2014**, *136*, 1718−1721.

(12) Dohner, E. R.; Jaffe, A.; Bradshaw, L. R.; Karunadasa, H. I. Intrinsic White-Light Emission from Layered Hybrid Perovskites. *J. Am. Chem. Soc.* **2014**, *136*, 13154−13157.

(13) Song, K. S.; Williams, R. T. *Self-Trapped Excitons*, 2nd ed.; Springer: Germany, 1996.

DOI: 10.1021/acs.jpclett.6b00793
J. Phys. Chem. Lett. 2016, 7, 2258−2263

(14) Yangui, A.; Garrot, D.; Lauret, J. S.; Lusson, A.; Bouchez, G.; Deleporte, E.; Pillet, S.; Bendeif, E. E.; Castro, M.; Triki, S.; et al. Optical Investigation of Broadband White-Light Emission in Self-Assembled Organic-Inorganic Perovskite $(C_6H_{11}NH_3)_2PbBr_4$. *J. Phys. Chem. C* **2015**, *119*, 23638−23647.
(15) Tomimoto, S.; Nansei, H.; Saito, S.; Suemoto, T.; Takeda, J.; Kurita, S. Femtosecond Dynamics of the Exciton Self-Trapping Process in a Quasi-One-Dimensional Halogen-Bridged Platinum Complex. *Phys. Rev. Lett.* **1998**, *81*, 417−420.
(16) Suemoto, T.; Tomimoto, S. Femtosecond Dynamics of Self-trapped Excitons in Quasi-One-Dimensional Halogen-Bridged Pt Complexes. *J. Lumin.* **1999**, *83*−*84*, 13−18.
(17) Wada, Y.; Lemmer, U.; Göbel, E. O.; Yamashita, M.; Toriumi, K. Time-Resolved Luminescence Study of Self-Trapped-Exciton Relaxation in Quasi-One-Dimensional Halogen-Bridged Mixed-Valence Metal Complexes. *Phys. Rev. B: Condens. Matter Mater. Phys.* **1995**, *52*, 8276−8282.
(18) Matsui, A.; Mizuno, K.; Tamai, N.; Yamazaki, I. Transient Free-Exciton Luminescence and Exciton—Lattice Interaction in Pyrene Crystals. *Chem. Phys.* **1987**, *113*, 111−117.
(19) Unuma, Y.; Masumoto, Y.; Shionoya, S.; Nishimura, H. Dynamical Aspects of Self-Trapping of *1s* Excitons in RbI and KI. *J. Phys. Soc. Jpn.* **1983**, *52*, 4277−4282.
(20) Emin, D. *Localization and Metal-Insulator Transition*; Plenum Publishing Corporation: New York, 1985.
(21) Kabanov, V. V.; Mashtakov, O. Y. Electron Localization with and without Barrier Formation. *Phys. Rev. B: Condens. Matter Mater. Phys.* **1993**, *47*, 6060−6064.
(22) Emin, D.; Holstein, T. Adiabatic Theory of an Electron in a Deformable Continuum. *Phys. Rev. Lett.* **1976**, *36*, 323−326.
(23) Morrissey, F. X.; Mance, J. G.; Pelt, A. D. V.; Dexheimer, S. L. Femtosecond Dynamics of Exciton Localization: Self-Trapping from the Small to the Large Polaron Limit. *J. Phys.: Condens. Matter* **2013**, *25*, 144204.
(24) Ishihara, T.; Takahashi, J.; Goto, T. Optical Properties Due to Electronic Transitions in Two-Dimensional Semiconductors $(C_nH_{2n+1}NH_3)_2PbI_4$. *Phys. Rev. B: Condens. Matter Mater. Phys.* **1990**, *42*, 11099−11107.
(25) Hu, T.; Wittenberg, J. S.; Lindenberg, A. M. Room Temperature Stabilization of Nanoscale Superionic Ag_2Se. *Nanotechnology* **2014**, *25*, 415705−415709.
(26) Ostroverkhova, O.; Cooke, D. G.; Shcherbyna, S.; Egerton, R. F.; Hegmann, F. A.; Tykwinski, R. R.; Anthony, J. E. Bandlike Transport in Pentacene and Functionalized Pentacene Thin Films Revealed by Subpicosecond Transient Photoconductivity Measurements. *Phys. Rev. B: Condens. Matter Mater. Phys.* **2005**, *71*, 035204.
(27) Sher, M.; Simmons, C. B.; Krich, J. J.; Akey, A. J.; Winkler, M. T.; Recht, D.; Buonassisi, T.; Aziz, M. J.; Lindenberg, A. M. Picosecond Carrier Recombination Dynamics in Chalcogen-Hyperdoped Silicon. *Appl. Phys. Lett.* **2014**, *105*, 053905.
(28) Kaindl, R. A.; Hägele, D.; Carnahan, M. A.; Chemla, D. S. Transient Terahertz Spectroscopy of Excitons and Unbound Carriers in Quasi-Two-Dimensional Electron-Hole Gases. *Phys. Rev. B: Condens. Matter Mater. Phys.* **2009**, *79*, 045320.
(29) Hegmann, F. A.; Lui, K. P. H. Optical Pump-Terahertz Probe Investigation of Carrier Relaxation in Radiation-Damaged Silicon-on-Sapphire. *Proc. SPIE* **2002**, *4643*, 31−41.
(30) Wu, X.; Trinh, M. T.; Niesner, D.; Zhu, H.; Norman, Z.; Owen, J. S.; Yaffe, O.; Kudisch, B. J.; Zhu, X. Trap States in Lead Iodide Perovskites. *J. Am. Chem. Soc.* **2015**, *137*, 2089−2096.
(31) Kobitski, A. Yu.; Zhuravlev, K. S.; Wagner, H. P.; Zahn, D. R. T. Self-Trapped Exciton Recombination in Silicon Nanocrystals. *Phys. Rev. B: Condens. Matter Mater. Phys.* **2001**, *63*, 115423.
(32) Vial, J. C.; Bsiesy, A.; Gaspard, F.; Herino, R.; Ligeon, M.; Muller, F.; Romestain, R.; Macfarlane, R. M. Mechanisms of Visible-Light Emission from Electro-Oxidized Porous Silicon. *Phys. Rev. B: Condens. Matter Mater. Phys.* **1992**, *45*, 14171−14177.
(33) Klafter, J.; Shlesinger, M. F. On the Relationship among Three Theories of Relaxation in Disordered Systems. *Proc. Natl. Acad. Sci. U. S. A.* **1986**, *83*, 848−851.
(34) Matsui, A.; Nishimura, H. Luminescence of Free and Self Trapped Excitons in Pyrene. *J. Phys. Soc. Jpn.* **1980**, *49*, 657−663.
(35) Solomon, E. I. Electronic Absorption Spectroscopy—Vibronic Coupling and Band Shape Analysis. *Comments Inorg. Chem.* **1984**, *3*, 300−318.
(36) Santomauro, F. G.; Lübcke, A.; Rittmann, J.; Baldini, E.; Ferrer, A.; Silatani, M.; Zimmermann, P.; Grübel, S.; Johnson, J. A.; Mariager, S. O.; et al. Femtosecond X-Ray Absorption Study of Electron Localization in Photoexcited Anatase TiO_2. *Sci. Rep.* **2015**, *5*, 14834.
(37) Mannebach, E. M.; Li, R.; Duerloo, K.-A.; Nyby, C.; Zalden, P.; Vecchione, T.; Ernst, F.; Reid, A. H.; Chase, T.; Shen, X.; et al. Dynamic Structural Response and Deformations of Monolayer MoS_2 Visualized by Femtosecond Electron Diffraction. *Nano Lett.* **2015**, *15*, 6889−6895.

DOI: 10.1021/acs.jpclett.6b00793
J. Phys. Chem. Lett. 2016, 7, 2258−2263